Astron. Astrophys. 183, 217–227 (1987)

ASTRONOMY
AND
ASTROPHYSICS

A study of the elongation of Abell clusters

I. A sample of 37 clusters studied earlier by Binggeli and Struble & Peebles

G.F.R.N. Rhee and P. Katgert

Leiden Observatory, P.O. Box 9513, 2300 RA Leiden, The Netherlands

Received November 13, 1986; accepted February 20, 1987

Summary. We present measurements of the elongation of the projected galaxy distributions in 37 Abell clusters clusters, all with redshifts less than or equal to 0.1. The measurements are based on the brightest 100 galaxies in each cluster. These are found with a semiautomated procedure which selects the n brightest, clearly non-stellar objects on digitized images of Palomar Sky Survey plates of the cluster areas.

The amplitude and position angle of the elongation signal (the "mirror-symmetric" component in the galaxy distribution) are found by Fourier analysis of the azimuthal distribution of the cluster galaxies. We also determine the statistical uncertainties of these parameters.

Comparison with earlier determinations of the elongation of these same clusters shows that the differences between independent position angle estimates *increase* with *decreasing* elongation amplitude. This explains most if not all of the previously reported apparent discrepancies between independent measurements.

The present data confirm that on average, clusters and their first ranked galaxies are very well aligned; there is also some, but as yet not conclusive evidence in our data for the reality of the Binggeli effect. The evidence, "pointing" of neighbouring clusters towards each other, is most convincing for the clusters with the strongest elongation signal.

Key words: Cosmology – clusters of galaxies – elliptical galaxies – formation of galaxies – image processing

1. Introduction

This article presents a study of the shape of 37 Abell clusters. The problem we wish to address is that of the origin of the structures on supercluster scales. The basic aim of this research is to answer an observational question concerning directional correlation of cluster orientations on scales up to ~ 100 Mpc ($H_0 = 50$ km/s/Mpc).

Binggeli (1982) has studied the shape and orientation of clusters of galaxies taken from the Abell Catalogue for which redshifts were known at that time. He found that out to distances of $30 \sim 40$ Mpc *neighbouring clusters appeared to point to each other*. In other words, he found that cluster major axes are not distributed randomly with respect to the direction towards their nearest neighbours. He even found some evidence for orientation correlation on scales up to 100 Mpc.

Binggeli was the first to find evidence for the statistical reality of such an effect. Clear evidence for a close correspondence between the position angles of cluster major axes and the orientation of the supercluster chains in which they are situated had been noted previously in the Coma and Perseus superclusters, see e.g. Oort (1983), and references therein. In these superclusters the principal clusters are rather convincingly aligned with the main supercluster branch.

Binggeli's result was recently questioned by Struble and Peebles (1985). They used a larger sample and *did not find such a directional correlation* at all and therefore concluded that Binggeli's result was a statistical mishap. Struble and Peebles found rather large differences between the position angles they obtained for 27 clusters for which Binggeli also quoted a position angle.

The aim of this article is to study the cause for this apparent disagreement, and to define methods that will give unambiguous results for elongation and elongation direction of clusters, taking into account the statistical uncertainties. This is a first but very important step in the process of confirming or refuting the Binggeli effect, which constitutes a prime test for theories of the formation of (large scale) structure in the universe.

2. A semi-automated method for galaxy detection on Palomar Sky Survey plates

In order to try and understand the disagreement between the results of Binggeli and Struble & Peebles we have developed an alternative method for studying the elongation of Abell clusters. Before we describe our method we first briefly describe Binggeli's method for obtaining position angles, and Struble & Peebles' method.

Binggeli proceeded as follows. First an approximate cluster center was defined; in most cases this was identified with the first ranked galaxy. Around this center a circle of radius

$$1.025 \times \frac{(1+z)^2}{z(1+z/2)} \text{ mm}$$

was drawn on a transparent overlay. This corresponds to a radius of 2 Mpc on the Palomar Sky Survey plates, or two thirds of the Abell radius (assuming $q_0 = 0$ and $H_0 = 50\,\text{km}\,\text{s}^{-1}\,\text{Mpc}^{-1}$). Within such a circle the 50 brightest galaxies were marked, ex-

Send offprint requests to: G.F.R.N. Rhee

cluding bright foreground galaxies. The cluster center was then recalculated as the arithmetic mean of the rectangular coordinates of the cluster galaxies. The straight line through the *new* center with

$$\sum_{i=1}^{50} b_i = \text{Minimum},$$

where b_i is the perpendicular distance of the ith cluster galaxy from the line, determines the cluster major axis.

Struble and Peebles determined position angles of clusters by visual inspection of Palomar Sky Survey prints. Each cluster was measured three times: print upright, inverted, and again upright, the quoted position angle is the mean of these three measurements.

In view of the discrepancy between the results of Binggeli and Struble & Peebles we decided to find a more objective method for determining position angles of clusters. The method consists of two parts. The first one is the selection of (cluster) galaxies from (Palomar Sky Survey) plates. The second one is the determination of elongation and elongation direction from the observed galaxy distribution.

In order to arrive at an objective method for finding cluster galaxies and their positions we decided to scan Palomar Sky Survey plates using the Leiden Astroscan automatic plate measuring machine. We used this machine to scan the PSS plates in regions around clusters for which both Binggeli and Struble & Peebles have data. We shall first describe the scanning method and shall then describe the three stages one must go through to reduce the digitised image to a list of candidate galaxies.

2.1. *Scanning method*

The plates were scanned using the Leiden Astroscan plate measuring machine. This is a computer controlled microdensitometer capable of producing a two dimensional digital photographic density map from a photographic plate. The machine has been described by Swaans (1981).

It works on the following principle. A small strip on the photographic plate is illuminated by a tungsten halide lamp and transmission through the plate is measured by a 128 element Reticon photodiode array. This transmission is translated into photographic density. The projected diode separation on the plate is 10 μ. The projected surface areas or beams of the detection diodes are of the order of 13 μm × 13 μm.

In order to deal with reasonably sized arrays of data, the fields to be scanned are subdivided into 1024^2 pixel arrays. We work with a 20 μ square aperture, (i.e. averaging the read-out of 4 10 μm × 10 μm pixels), in which case 1024 pixels correspond to a linear dimension of 2.048 cm or 23.1 arc minutes on the Palomar Sky Survey plate-scale. The offline reduction is then done for each 1024^2 array individually.

The first step in the data reduction is to find and subtract the local sky background. The second step consists in detecting all the objects in an array. The final step consists of classifying the objects as stars or galaxies. We shall now give a brief description of each of these steps.

2.2. *Finding the background*

We define the background as containing only photographic density fluctuations with spatial frequencies lower than a selected cutoff frequency. The initial array of data is divided into small equal square submatrices with sizes larger than those of most images but small enough to allow for relatively fast fluctuations in the background to be detected. The size of the submatrix used in our case is 64 by 64 pixels or 1.44 by 1.44 arc minutes on the Palomar Sky Survey plate-scale.

A histogram of the photographic densities in each submatrix is then computed. The wing of the histogram at low densities is the part least influenced by the objects present. It is this wing which is used to fit a gaussian as a model of the background.

Once the background values have been computed for each submatrix one interpolates these values to obtain a continuous smooth background map with the same dimensions as the original matrix. This map has a maximum spatial frequency equal to the cutoff frequency (in our case 1.44 arc minutes) and is subtracted from the original matrix.

2.3. *Object detection*

The next step in the reduction procedure consists in detecting the objects. The background subtracted map obtained in the manner described in the previous section has a flat background around zero density level on which object images are superimposed.

A threshold level is defined on this resulting matrix. The matrix is then clipped at this level. This threshold is defined in terms of the noise, in photographic density, in the background averaged over the whole matrix. Each group of one or more adjacent pixels with densities above the threshold level is considered to be a separate object.

In order to deal with merged objects the matrix is clipped at 4 different threshold levels, starting at high density and going down to the 3σ level. The 3σ level is defined as the plate limit. During this process several parameters are stored for each object. The two parameters relevant for the present study are object position and the object brightness. The object position is defined as the geometrical mean position of the detected object surface. The object brightness is defined as the sum of the object intensities (derived from the photographic densities using an assumed characteristic curve) over an area proportional to the number of pixels above the 3σ level. The area has a minimum size of 7 by 7 pixels (140 μm on a side, or 9.4″) and a maximum size of 30 by 30 pixels (~40″ by 40″).

2.4. *Star/galaxy separation*

Having detected all the objects down to a certain minimum threshold level in photographic density, the next stage involves separating the stellar from non-stellar objects. The separation criterion we used was based on that devised by Kron (1980).

Using the density matrix of an object we calculate two further parameters. The object position is redefined as the mean position of the five brightest pixels of the nine pixels surrounding the first object position (the geometrical mean). We then calculate the first moment of the object image as follows

$$(r_{-1})^{-1} = \frac{\sum I(x,y)/r}{\sum I(x,y)}$$

r is defined as the integer truncated distance from the central object position, and $I(x,y)$ is the relative intensity of pixel (x,y).

One problem arises when working with the Sky Survey plates, namely that one does not know very well the characteristic curve

of the emulsion. Minkowski and Abell (1963) have noted that the photographic contrasts for these emulsions ranged between 1.5 and 2.0. Since we do not know the characteristic curve of an individual plate we have to assume an average γ. We then convert from a difference in photographic density (i.e. the density above the background) to a ratio of intensities using the relation

$$(I - I_b)/I_b = 10^{(D - D_f)/\gamma} - 1$$

This assumes a single γ across an object i.e. from background to maximum density. This assumption breaks down if the plate is very thinly exposed and the sky background is still in the toe of the characteristic curve, or where the plate is saturated. The $D - \log I$ relation is then not linear, and a single γ does not apply. Assuming a constant γ at low density means that we overestimate the intensity at the faintest levels of a thinly exposed plate.

Having calculated the r_{-1} parameter a diagram is then plotted of this parameter versus object magnitude. The object magnitude is defined as $-2.5\log(I)$ where I is the object brightness as defined in Sect. 2.3. It is this diagram which we use to discriminate between stars and galaxies (see Fig. 1). Using 40 objects (20 stars and 20 galaxies) classified by eye the position of a line separating stars from non-stellars (assumed to be all galaxies) is determined. All objects above this line (i.e. with $1/r_{-1}$ larger than the minimum value for its brightness) are defined as non-stellar, i.e. galaxies, We wish to make clear that this is a semi-automated method. In practice it works as follows. A grey scale plot of each matrix is made which is effectively a 10 times enlargement of a 2 by 2 cm area on the Sky Survey. For each greyscale plot two overlay plots are generated with positions and sequence numbers of detected objects. The first overlay plot contains all the detected objects down to a certain 'magnitude' threshold (well above the surface brightness 3σ cut-off). This plot enables one to obtain parameters for any object on the greyscale plot. The second overlay plot contains only the candidate galaxies and is used to check if these objects are indeed galaxies.

We believe that with this method we can reliably determine the positions of the 100 brightest galaxies in Abell clusters of richness class greater than or equal to 1 and redshift less than or equal 0.1.

3. Measuring cluster elongation amplitude and direction

We now turn to the next major step in the analysis, namely the method for determining cluster elongation direction from a two dimensional distribution of galaxies. We exclude the very brightest and obviously unrelated galaxies.

Before we describe our method, we want to stress the importance of being able to announce the significance of an individual direction estimate.

One does not have as yet a confirmed model for the surface density of galaxies in Abell clusters. This problem is clearly illustrated by the figures in Geller and Beers (1982); there does not appear to be a simple density distribution model valid for all clusters. We thus devised an approach which allows us to test for mirror symmetry while making a minimum number of assumptions about the galaxy distribution.

The drawbacks of the methods used to date (outlined in Sect. 2) is that they do not quote a signal strength. Binggeli gives an ellipticity but this is not quoted for all the clusters for which he gives position angles. It is also not quantified to what extent substructure influences the position angles as determined by Binggeli and Struble & Peebles.

We decided to derive not only position angles of cluster elongation, but also a "signal strength" of any mirror-symmetry in the galaxy distributions as well as the associated statistical uncertainties in both parameters. The method used is described in Sect. 3.1.

The elongation parameter is calculated as follows. First the n brightest galaxies within a 2 Mpc radius of the cluster center are selected. The cluster center is defined initially as the position of

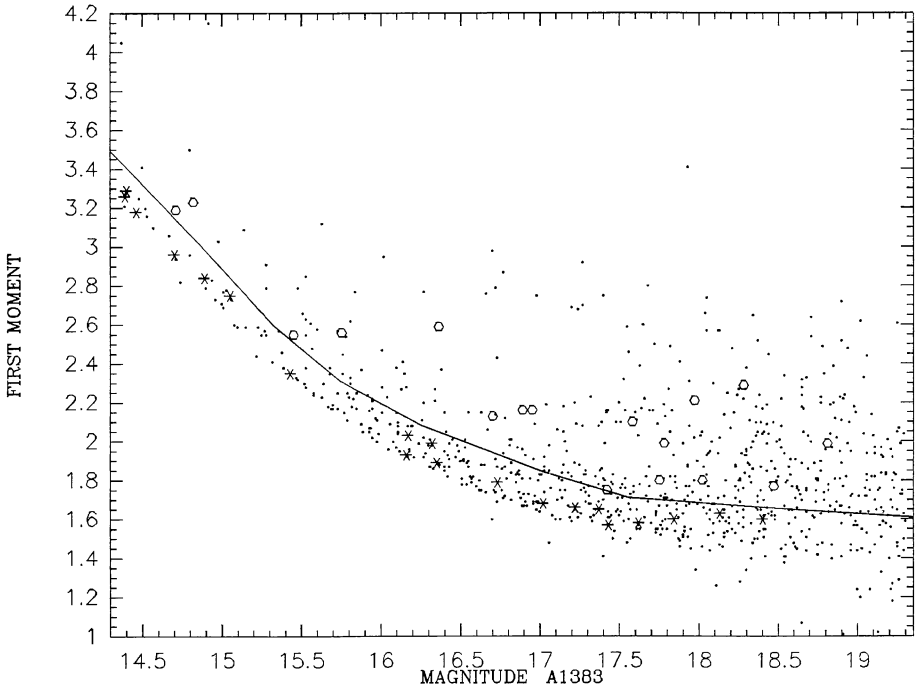

Fig. 1. Plot of the effective radius parameter ($1/r_{-1}$) versus magnitude for objects detected in a 4 by 4 cm area scanned centered on the cluster Abell 1383. The magnitude scale is roughly calibrated using Abell's estimate for the 10th brightest cluster member. The line is drawn using 20 stars and 20 galaxies chosen by eye. The stars used are shown as six-pointed stars and the galaxies used are shown as pentagons in the figure. The line is used to eliminate the obvious stellar objects which are below the line. The remaining objects (above the line) are then checked by eye

the first ranked galaxy. A new center is then defined by taking the arithmetic mean of the coordinates of the n brightest cluster galaxies (where n varies between 50 and 100). The n brightest galaxies within a 2 Mpc radius of the new center are finally selected to define the galaxy distribution. The determination of the cluster center is important to the Fourier analysis described in the following section. To check that the cluster center we found was reliable we checked the amount that the cluster center had moved during the iterations described above. We found that the new cluster center position did not vary by more than 5% of the cluster diameter during the analysis described above.

3.1. *Fourier analysis of the azimuthal galaxy distribution in a cluster*

Having calculated the center of the galaxy distribution as described in Sect. 3, we determine the position angle of each galaxy with respect to the center. The azimuthal galaxy distribution is obtained by binning the galaxies (this is not essential) in N_i bins where ϕ_i is the position angle of the ith bin. From the binned distribution we calculate four parameters: S, C, N_1 and ϕ_0. S is the π sine fourier component and C is the π cosine fourier component. N_1 and ϕ_0 are calculated with the following model for the azimuthal galaxy distribution in mind;

$$N(\phi) = (N_0/2\pi)[1 + (N_1/N_0)\cos(2\phi - 2\phi_0)]$$

ϕ is the azimuthal angle

ϕ_0 is the angle defining the axis of mirror symmetry of the cluster

N_0 is the normalising parameter corresponding to the total number of galaxies in the cluster $N_0 = \int N(x)\,dx$

N_1 is the elongation amplitude of the distribution. For a distribution of this kind our derived ϕ_0 and N_1 are identical to ϕ_0 and N_1 of the model. For the $\sin(2\phi)$ and $\cos(2\phi)$ fourier components we obtain:

$$S = (N_1/2)\sin 2\phi_0\,, \qquad C = (N_1/2)\cos 2\phi_0$$

thus $N_1 = 2(S^2 + C^2)^{1/2}$ and $\phi_0 = \frac{1}{2}\arctan(S/C)$. Using the definition of S and C we can derive the statistical uncertainties in N_1 and ϕ_0. When $N_1/N_0 \ll 1$, which is the case if the signal to noise in N_1 is marginal, we have $\sigma^2_{N_i} \sim N_0/N_b$ (N_b is the number of bins). This leads to $\sigma_s = \sigma_c \sim (N_0/2)^{1/2}$, thus $\sigma_{N_1} = (2N_0)^{1/2}$ and $\sigma_{\phi_0} = (\frac{1}{2}\sigma_{N_1}/N_1)$. With a realistic signal σ_{N_1} and σ_{ϕ_0} probably underestimate the real uncertainties by an amount which depends on N_1. Note that σ_{N_1} depends only on N_0 while σ_{ϕ_0} depends only on N_1/σ_{N_1}.

For a given cluster, N_1/σ_{N_1} depends on four factors: the intrinsic amount of elongation of the cluster, the number of galaxies used to detect the elongation, the amount of substructure and, the amount of contamination by noncluster galaxies. Therefore, low values of N_1/σ_{N_1} will result for perfectly axisymmetric galaxy distributions (no matter how many galaxies are used to detect an elongation). Elongated galaxy distributions containing either a small number of galaxies, or a lot of substructure superimposed on an assumed "mirror-symmetric" distribution will also produce low values of N_1/σ_{N_1}, as will clusters which have small contrast with respect to the background.

For our present purpose, the reason for an individual low value of N_1/σ_{N_1} is less important than the realisation that clusters with low values of N_1/σ_{N_1} should enter "alignment tests" with much lower weight than clusters with high values of N_1/σ_{N_1}.

3.2. *Internal consistency*

In order to convince the reader of the applicability of the analysis described above, we shall compare the position angle uncertainties derived from the model described above with position angle uncertainties derived from the data.

To estimate the uncertainty in cluster position angle from our data we calculate the position angle for a cluster using two independent galaxy distributions. We calculate the signal strength and position angle using 50 galaxies selected from the hundred brightest arranged in order of decreasing brightness. Firstly we choose the 50 "even numbered" galaxies (i.e. the second fourth sixth brightest galaxy up to the faintest of the hundred. We do the same for the "odd numbered" galaxies. In this way we come as close as we can to producing two independent equivalent determinations of the structure of an individual cluster. We then calculate the signal strengths and position angles from these samples which in principle provide independent estimates of the structure of one underlying distribution. The resulting strengths and position angles are listed in Table 4. 50e refers to the results calculated from the fifty "even" galaxies and 50o refers to the results calculated from the fifty "odd" galaxies. One can estimate a single value of $\sigma_\phi(\text{data})/\sigma_\phi(\text{model})$ from the distribution of the parameter $\Delta\phi/\sigma_c = (\phi_e - \phi_o)/(\sigma^2_{\phi_e} + \sigma^2_{\phi_o})^{1/2}$. If $\sigma_\phi(\text{data})/\sigma_\phi(\text{model}) = 1$ the parameter defined above will be normally distributed with mean 0 and dispersion 1. The 37 clusters in this sample give a distribution of $\Delta\phi/(\sigma^2_{\phi_e} + \sigma^2_{\phi_o})^{1/2}$ with a mean of 0.01 and a dispersion of 1.28 with a shape which is very close to gaussian (see Fig. 2). 68% of the values fall within ± 1.20 and 95% of the pairs within ± 2.0.

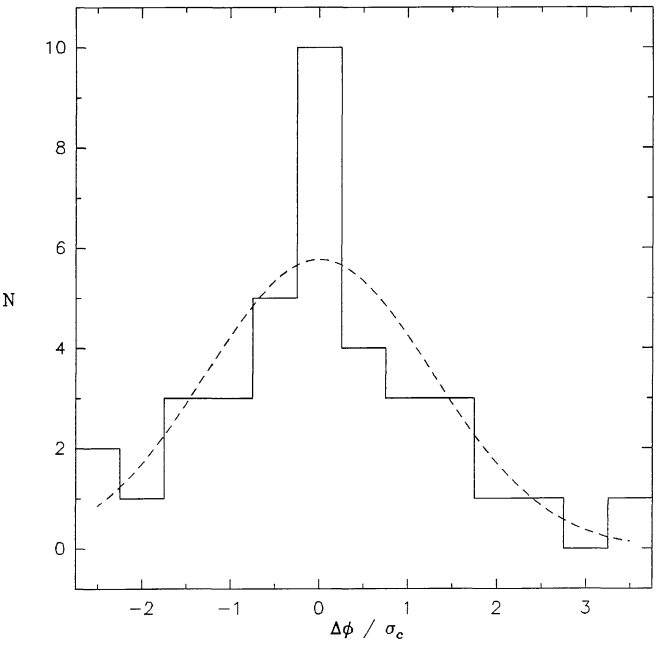

Fig. 2. As described in Sect. 3.2, we calculate ϕ_e, σ_{ϕ_e}, ϕ_o, σ_{ϕ_o} using the 50 "odd numbered" galaxies and the 50 "even numbered" galaxies chosen from the brightest 100. For each cluster we then calculate $(\phi_o - \phi_o)/(\sigma^2_{\phi_e} + \sigma^2_{\phi_o})^{1/2}$. These values are shown in histogram form in the figure. The dashed line shows a gaussian profile with a mean of 0.01 and a dispersion of 1.28. The gaussian is normalised to 37; the number of clusters on the histogram

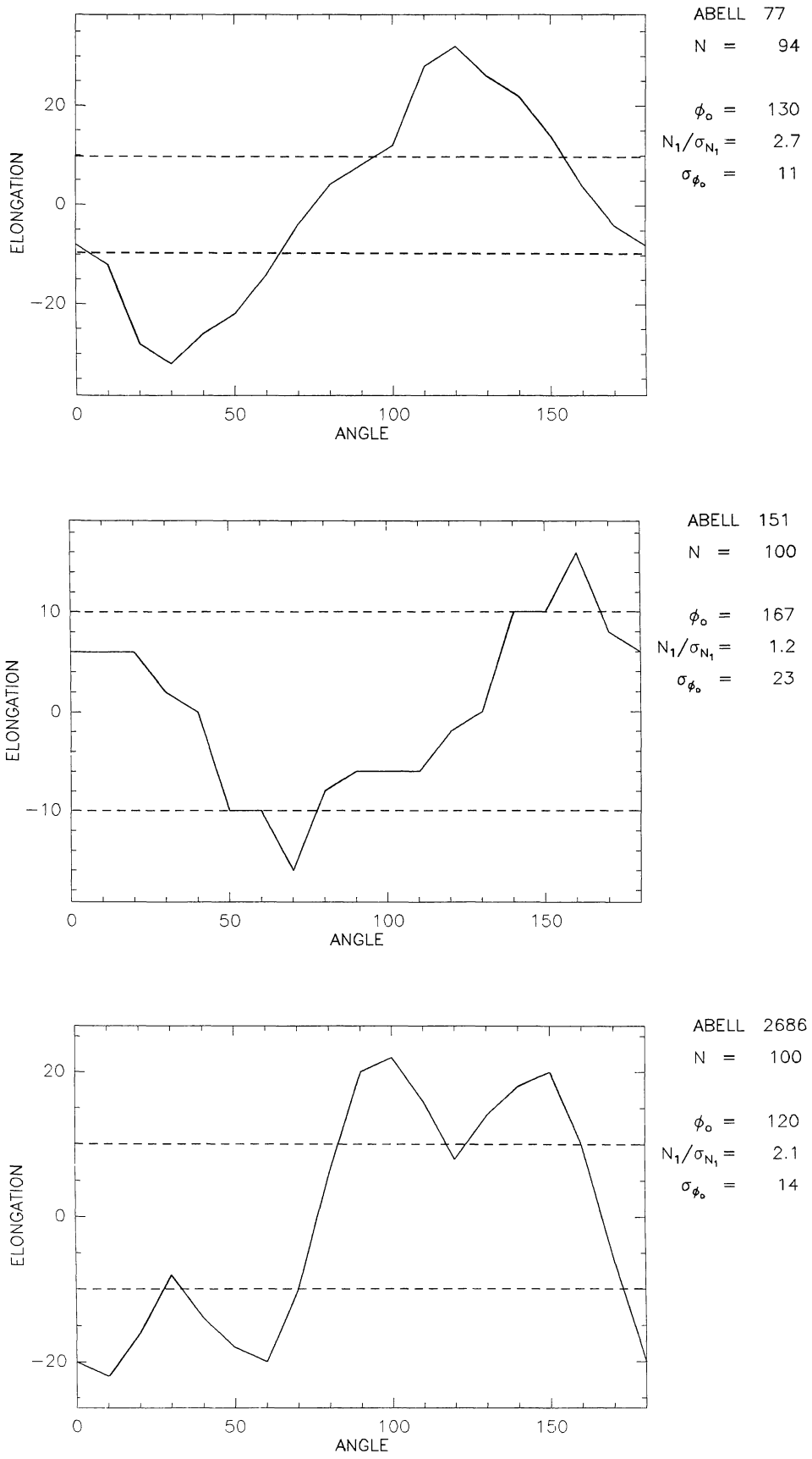

Fig. 3a–c. Elongation statistic (see Sect. 3.3) versus position angle for the clusters **a** Abell 77, **b** Abell 151 and **c** Abell 2686. N is the number of galaxies used, ϕ_o is the position angle of the cluster, σ_{ϕ_o} is the estimated error in position angle, N_1/σ_{N_1} is the signal strength (defined in Sect. 3.1)

3.3. The elongation statistic

In order to get a feel for the presence of angular substructure in the cluster we calculate an "elongation signal" as a function of position angle; this is also useful as a visual check of the fourier transform result. One first calculates the cluster center as in the previous method and then divides the cluster area into four quadrants. One then calculates the sum of the number of galaxies in opposing quadrants and the elongation statistic is defined as the difference between these two sums. In other words if the number of galaxies in the four quadrants is Q_1, Q_2, Q_3, Q_4 respectively then the elongation statistic is $\varepsilon = (Q_1 + Q_3) - (Q_2 + Q_4)$. This statistic seems (intuitively) to be close to optimal for detecting mirror symmetry. One can calculate this statistic for several position angles. The use of this statistic is that it gives one an idea of the angular substructure in the cluster.

The data we obtain for the cluster Abell 151 indicate that the large disagreement between Binggeli and Struble and Peebles is due to the fact that only a weak signal is present, as shown in Fig. 3b. Figure 3a shows the data obtained for Abell 77, not surprisingly the position angles quoted by Binggeli and Struble and Peebles for this cluster agree to 10°. The data for Abell 2686 (Fig. 3c) are closer to Struble and Peebles' quoted position angle than to Binggeli's but the signal is not very strong. Figure 3c also indicates that substructure is present and this may have influenced the position angle determinations of Binggeli and Struble & Peebles.

4. Results

Using the methods described in Sect. 3 a sample of 37 Abell clusters were scanned with the Leiden Astroscan machine. The basic scanning unit is a matrix of 1024^2 20 μm pixels. This corresponds to a size of ~ 2 by 2 cm on the Palomar Sky Survey prints, or 22.9 by 22.9 arcmin. The number of matrices scanned for a cluster is determined by the criterion that an area with a radius of at least

$$1.025 \times \frac{(1+z)^2}{z(1+z/2)} \text{ mm is digitized}$$

This corresponds to 2 Mpc at the cluster redshift.

We present our results in Table 1. Column 1 gives the cluster name, column 2 the cluster redshift. For each cluster the number of galaxies is varied from 50 to 100 (column 3). The radius within which these galaxies are selected was varied from $2 \sim 3$ Mpc (column 4). Column 5 gives our position angle. In column 6 we quote the signal strength (intensity parameter divided by its standard deviation see Sect. 2). Note that the scanning method determines by how much we can vary the radius parameter.

Our final cluster position angle is determined using the 100 brightest galaxies (excluding obvious field galaxies) within a 2 Mpc radius (see Table 2).

4.1. Comparison of our results with those of Binggeli and Struble & Peebles

To assess how the position angle differences vary as a function of signal strength Figs. 4a, 4b and 4c show plots of the difference in position angle versus the strength of the signal we used to obtain our position angle. Figure 4a compares Binggeli's data with those of Struble and Peebles, figure 4b compares our data with those of Struble and Peebles, figure 4c compares our data with those of Binggeli.

Trends of decreasing $\Delta\phi$ with increasing N_1/σ_{N_1} are clearly visible. In order to quantify these trends the data are binned in N_1/σ_{N_1}. We then calculate the mean of the absolute value of differences in position angle for the data in each bin. The results are shown in Table 3.

Figures 4d, 4e, 4f illustrate the results of Table 3. The differences in position angle as measured by the three different methods decrease as the signal strength increases. This enables us to estimate the accuracy of a given position angle. This is essential for subsequently assessing the statistical significance of any effect we may find

Struble and Peebles and Binggeli have 27 clusters in common. For these clusters Struble and Peebles quote a $\Delta = 6.1°$, $\sigma_\Delta = 42.8°$. Struble & Peebles find that this large dispersion is due to three clusters A 151, A 154, and A 2142 having $|\Delta| \simeq 90$. They find that if these clusters are excluded $\Delta = 1.5°$, $\sigma_\Delta = 28.5°$. The data quoted by Binggeli for the cluster Abell 154 were taken from Carter and Metcalfe (1981).

4.2. The alignment of clusters and first ranked galaxies

Sastry (1968) was the first to show that first ranked galaxies tend to have an orientation that is very similar to that of their surrounding cluster. This alignment has been confirmed in many cluster studies (e.g. Dressler, 1981). This effect appeared strongest in the study of Carter and Metcalfe (1981): for all but one in their sample of 14 clusters the difference between the cluster and the first ranked galaxy (major-axis) position angle is less than 30°. Binggeli (1982) also found such an effect in his data. Binggeli found that the effect was strongest for clusters having Bautz-Morgan class less than or equal to II.

In Fig. 5 we plot the absolute frequency distribution of the difference between cluster position angle and the position angle of the first ranked galaxy. We confirm the result that clusters and their first ranked galaxies tend to have very similar orientations on the sky.

Argyres et al., (1986) have found that Lick galaxy counts are systematically high along the line defined by the long axis of a cluster or its dominant member. The effect extends out to at least 30 Mpc from the clusters. This suggests that the position angle of the brightest cluster member is related to 30 Mpc structure.

4.3. Preliminary check of the Binggeli effect

Using our data for the position angles of 37 clusters we have applied Binggeli's test for cluster alignment. The test is performed as follows; Our list of cluster redshifts is taken from Binggeli (1982) Table 3. The spatial location of each cluster is calculated from the cluster's right ascension declination and redshift, Euclidean geometry is assumed. For each of the 37 clusters listed in Table 2 we find the spatially closest neighbour: this neighbour is not necessarily listed in Table 2 but is certainly in Binggeli's Table 3. The projected connecting line along a great

Table 1. Column 1 Abell number, column 2 redshift (from Binggeli (1982)), column 3 number of galaxies used to determine position angle, column 4 radius in Mpc within which N brightest galaxies were selected, column 5 position angle, column 6 signal strength N_1/σ_{N_1}

Abell	Redshift	N_{gal}	Radius (Mpc)	ϕ_{RK}	N_1/σ_{N_1}	Abell	Redshift	N_{gal}	Radius (Mpc)	ϕ_{RK}	N_1/σ_{N_1}
77	0.0900	50	1.9	123	3.7	1773	0.0776	50	2.0	15	3.4
		100	1.9	125	2.1			100	2.0	52	1.2
		50	3.4	103	2.8			100	2.4	40	1.5
85	0.0518	50	2.0	144	1.6	1775	0.0718	100	1.8	145	1.8
		100	2.0	140	2.2			50	2.3	136	1.6
		50	2.7	158	3.1			100	2.3	136	1.5
		100	2.7	166	1.7	1795	0.0621	50	2.0	6	2.1
119	0.0440	50	2.0	9	0.2			100	2.0	22	3.0
		100	2.0	33	0.7	1809	0.0788	50	2.5	59	2.2
		100	2.3	46	1.3			100	2.5	41	2.6
151	0.0526	50	2.0	146	0.7	1831	0.0733	50	1.9	172	1.2
		100	2.0	167	1.2			100	1.9	156	1.7
		50	2.7	37	1.4			100	2.4	171	2.0
		100	2.7	150	0.8	1837	0.0650	50	2.0	33	2.5
193	0.0610	50	2.0	59	1.5			100	2.0	14	1.7
		100	2.0	37	0.8	1991	0.0586	50	2.1	26	3.6
225	0.0692	50	2.0	77	1.7			100	2.1	19	4.7
		100	2.0	74	4.5	2029	0.0767	50	2.0	162	1.6
		50	2.3	67	3.2			100	2.0	156	1.3
		100	2.3	51	0.6			100	2.4	131	1.3
401	0.0748	50	2.0	28	2.0	2061	0.0768	50	2.0	179	0.6
		100	2.0	35	3.0			100	2.0	47	0.6
		100	2.6	22	2.4			100	2.5	45	1.9
496	0.0360	50	1.9	3	0.5	2079	0.0662	50	2.0	46	2.1
		100	1.9	128	1.1			100	2.0	38	1.8
514	0.0731	50	2.1	148	1.5	2089	0.0743	50	2.0	100	1.8
		100	2.1	118	1.8			100	2.0	94	2.4
		100	2.4	117	1.9			100	2.5	110	2.7
978	0.0527	50	1.9	156	3.4	2107	0.0421	50	2.0	160	0.9
		100	1.9	161	4.4			100	2.0	93	0.9
1185	0.0349	50	1.1	90	2.6	2124	0.0640	50	2.2	180	1.2
		100	1.1	111	2.7			100	2.2	165	0.9
1187	0.0791	50	2.0	53	2.8	2142	0.0904	50	2.3	119	1.5
		100	2.0	69	3.2			100	2.3	145	2.4
1190	0.0900	50	2.0	162	1.1			50	2.9	132	1.4
		100	2.0	168	2.2			100	2.9	148	1.3
		100	3.1	166	3.0	2151	0.0371	50	1.9	56	2.2
1228	0.0440	50	1.9	117	1.0			100	1.9	47	1.7
		100	1.9	140	1.6	2175	0.0978	50	2.4	132	0.9
1383	0.0603	50	2.0	139	2.4			100	2.4	131	3.0
		100	2.0	135	1.5			100	3.0	124	2.3
1644	0.0453	50	2.0	160	1.6	2256	0.0601	50	2.0	124	2.1
		100	2.0	10	2.2			100	2.0	113	2.8
1691	0.0722	50	2.0	132	1.0	2457	0.0597	50	2.0	52	1.3
		100	2.0	157	0.5			100	2.0	80	1.1
1767	0.0701	50	2.0	157	2.5	2686	0.1000	50	2.1	117	1.5
		100	2.0	1	0.5			100	2.1	115	1.6
		100	2.5	175	2.1			100	3.0	135	3.5

Table 2. Comparison of results of Rhee & Katgert, Binggeli, Struble & Peebles. Column 1 Abell number, column 2 our cluster p.a. this paper, column 3 cluster p.a. from Binggeli, column 4 cluster p.a. from Struble & Peebles, column 5 difference between our data and the Binggeli data, column 6 difference between our data and the Struble & Peebles data, column 7 difference between Binggeli's data and Struble & Peeble's data. Column 8 shows the elongation strength used to determine the cluster p.a. Column 9 gives the position angle of the first ranked galaxy taken from Binggeli (1982)

Abell	ϕ_{RK}	ϕ_B	ϕ_{SP}	$\Delta\phi_{RK-B}$	$\Delta\phi_{RK-SP}$	$\Delta\phi_{B-SP}$	N_1/σ_{N_1}	f,r. gal
77	125	110	105	15	20	5	2.1	108
85	140	150	155	−10	−15	−5	2.2	140
119	33		25		8		0.7	37
151	167	112	23	55	−36	89	1.2	35
193	37	46	130	−9	87	−84	0.8	
225	74		51		23		4.5	88
401	35	39	40	−4	−5	−1	3.0	31
496	128	99	148	29	−20	−49	1.1	176
514	118		115		3		1.8	7
978	161	171	160	−10	1	11	4.4	
1185	111	157	176	−46	−65	−19	2.7	39
1187	69		96		−27		3.2	101
1190	168	176	126	−8	−42	50	2.2	1
1228	140		68		72		1.6	36
1383	135		158		−23		1.5	156
1644	10	176	170	14	20	6	2.2	47
1691	157	178	149	−21	8	29	0.5	159
1767	1	12	37	−11	−36	−25	0.5	148
1773	52	18	32	34	20	−14	1.2	34
1775	145	114	122	31	23	−8	1.8	125
1795	22	32	11	−10	−11	21	3.0	14
1809	41	49	54	−8	−13	−5	2.6	52
1831	156		161		−5		1.7	157
1837	14	12	20	2	−6	−8	1.7	47
1991	19	30	25	−11	−6	5	4.7	10
2029	156	37	26	−61	50	11	1.3	25
2061	47		32		15		0.6	44
2079	38		26		12		1.8	10
2089	94	107	114	−13	−20	−7	2.4	105
2107	93	62	137	31	−44	−75	0.9	116
2124	165	171	153	−6	12	18	0.9	154
2142	145	34	143	−69	2	71	2.4	131
2151	47	24	32	23	15	−8	1.7	36
2175	131	136	125	−5	6	11	3.0	151
2256	113	145	133	−32	−20	12	2.8	125
2457	80	33	67	47	13	−34	1.1	87
2686	115	167	115	−52	0	52	1.6	

Table 3. The mean of the absolute value of the position angle differences; the data are binned in N_1/σ_{N_1} (5 bins, bin width 1).
Column 1 N_1/σ_{N_1}, column 2 dispersion in position angle differences $\langle|\Delta\phi|\rangle_{RK-B}$, column 3 number of clusters used to calculate $\langle|\Delta\phi|\rangle_{RK-B}$, column 4 $\langle|\Delta\phi|\rangle_{RK-SP}$, column 5 N_{RK-SP}, column 6 $\langle|\Delta\phi|\rangle_{B-SP}$, column 7 N_{B-SP}

N_1/σ_{N_1}	$\langle\|\Delta\phi\|\rangle_{RK-B}$	N_{RK-B}	$\langle\|\Delta\phi\|\rangle_{RK-SP}$	N_{RK-SP}	$\langle\|\Delta\phi\|\rangle_{B-SP}$	N_{B-SP}
0.5	15.6	5	30.0	7	46.2	5
1.5	37.1	9	21.3	14	30.3	9
2.5	21.1	8	19.0	8	20.1	8
3.5	6.3	3	12.3	4	11.0	3
4.5	10.5	2	10.0	2	8.0	2

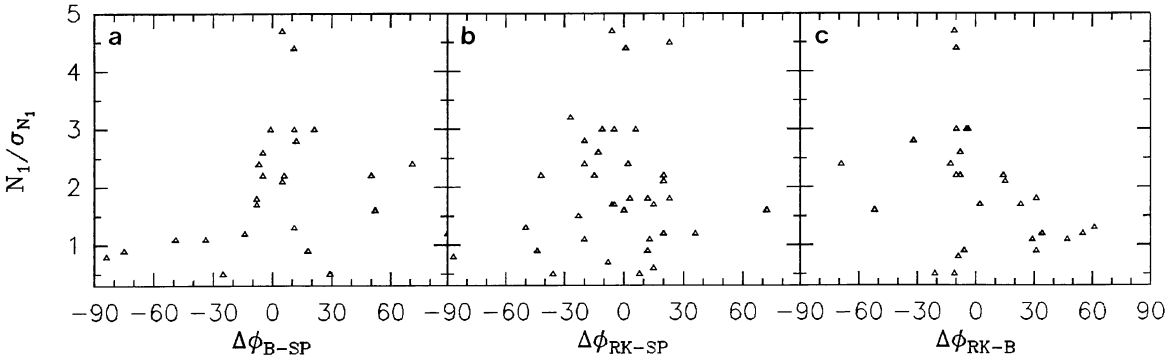

Fig. 4a–c. Difference in position angle as a function of signal strength (N_1/σ_{N_1}). **a** Binggeli-Struble & Peebles, **b** Rhee & Katgert-Struble & Peebles, **c** Rhee & Katgert-Binggeli

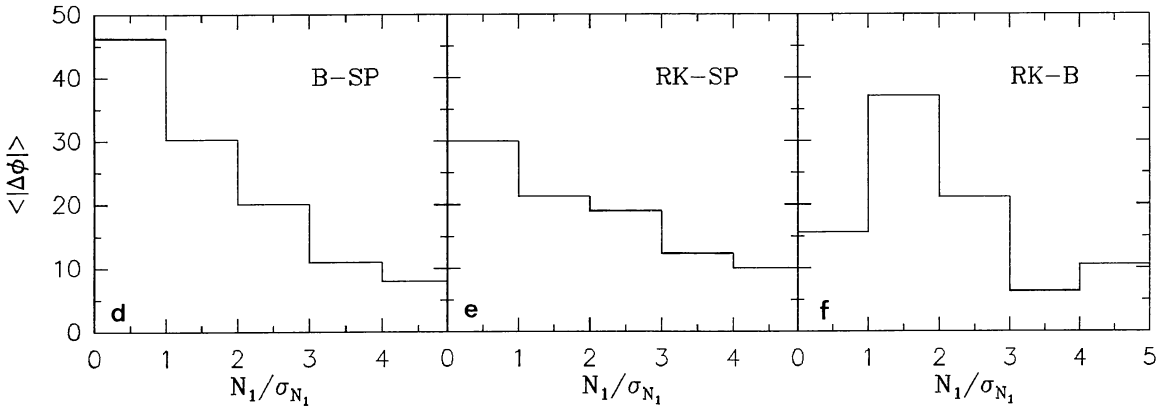

Fig. 4d–f. The mean absolute value of position angle differences binned in N_1/σ_{N_1}. **d** Binggeli-Struble & Peebles, **e** Rhee & Katgert-Struble & Peebles, **f** Rhee & Katgert-Binggeli

Table 4. Result of calculating position angle and signal strength using the 50 even numbered and 50 odd numbered galaxies selected from the 100 brightest. Column 1 Abell number of cluster, column 2 position angle using 50 'even' galaxies, column 3 N_1/σ_{N_1} calculated using the 50 'even' galaxies, column 4 position angle from 50 'odd' galaxies, column 5 N_1/σ_{N_1} calculated using the 50 'odd' galaxies, column 7 position angle different (column 2 minus column 4) divided by $\sigma_c = (\sigma^2_{\phi_o} + \sigma^2_{\phi_e})^{1/2}$

Abell	ϕ_{even}	N_1/σ_{N_1}(even)	ϕ_{odd}	N_1/σ_{N_1}(odd)	$\Delta\phi/\sigma_c$	Abell	ϕ_{even}	N_1/σ_{N_1}(even)	ϕ_{odd}	N_1/σ_{N_1}(odd)	$\Delta\phi/\sigma_c$
77	118	3.6	114	1.1	0.15	1775	141	1.7	123	1.0	0.54
85	143	1.8	139	0.9	0.11	1795	16	2.8	23	1.7	−0.36
119	157	1.0	36	1.2	−1.58	1809	23	1.6	52	2.7	−1.39
151	148	1.3	179	0.4	−0.41	1831	161	0.8	164	1.9	−0.08
193	46	2.0	121	1.1	−2.52	1837	55	1.1	179	2.2	1.92
225	82	2.8	65	3.2	1.25	1991	180	2.1	28	4.9	−1.89
401	30	0.5	38	3.2	−0.14	2029	155	0.6	131	1.5	0.47
496	63	1.3	171	2.0	2.74	2061	117	0.2	25	0.7	−0.59
514	136	1.8	99	1.6	1.54	2079	19	1.4	51	1.4	−1.11
978	156	3.0	158	3.2	−0.15	2089	86	1.8	90	1.1	−0.13
1185	88	1.4	124	2.1	−1.46	2107	84	2.2	177	1.3	3.40
1187	69	3.8	111	0.7	−1.01	2124	169	1.0	129	1.1	1.03
1190	5	1.7	163	2.0	0.99	2142	154	2.6	112	0.7	0.99
1228	126	0.7	152	1.7	−0.59	2151	59	0.7	31	1.6	0.63
1383	145	0.2	145	1.4	0.00	2175	127	3.2	132	0.8	−0.14
1644	2	1.5	15	0.6	−0.25	2256	125	1.6	96	2.2	1.31
1691	146	1.1	171	0.1	−0.09	2457	34	1.3	93	2.4	−2.35
1767	157	2.5	1	0.5	0.82	2686	123	1.3	106	0.7	0.37
1773	59	1.1	49	0.9	0.24						

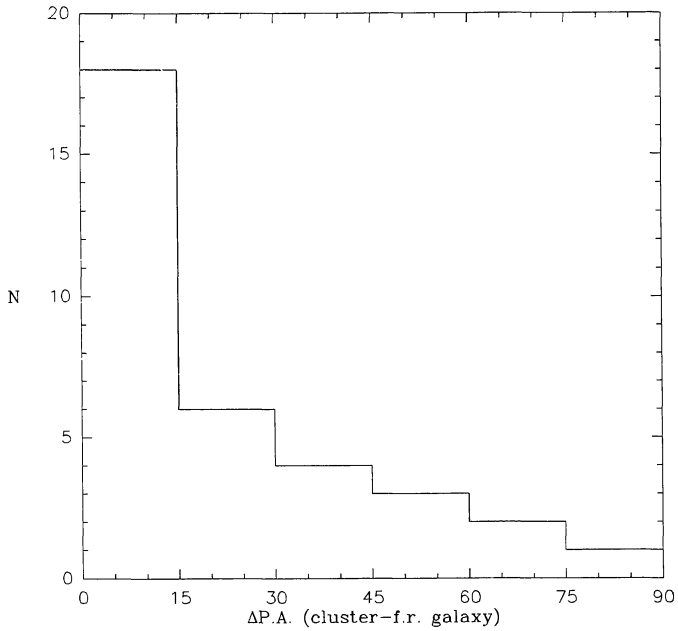

Fig. 5. The absolute frequency distribution of the difference between cluster position angle and position angle of the first ranked galaxy

circle on the sky between a pair of neighbouring clusters defines a position angle at the place of the primary cluster indicating the direction to its closest neighbour. These position angles are calculated by means of spherical trigonometry and are compared with the position angles of the cluster given in Table 2. Figure 6a shows the difference (θ) between the cluster position angle and the position angle defined by the direction to the closest neighbour versus the spatial distance (D) to the closest neighbour. Figure 6b shows the same plot as Fig. 6a with the symbol size for each cluster being proportional to the strength of elongation for that cluster. One gets a clear visual impression from this plot that an alignment is present on scales smaller than ~ 30 Mpc. In order to quantify this visual impression we calculate the parameter $\rho = (\phi_{cl} - \phi_n)/\sigma_\phi$ for each cluster. ϕ_{cl} is the cluster position angle, ϕ_n is the position angle defined by the direction to the nearest neighbour and σ_ϕ is the uncertainty in the cluster position angle. Using our 36 clusters we form 3 bins in distance containing 12 clusters each. We then calculate the mean ρ which we denote by μ and the root mean square ρ denoted by σ. For $0 \leq D \leq 32$ Mpc, we obtain $\mu = 0.28$, $\sigma = 2.63$. For $32 \leq D \leq 52.5$ Mpc, $\mu = 0.35$, $\sigma = 3.9$. For $52.5 \leq D \leq 133$ Mpc, $\mu = 1.55$, $\sigma = 3.98$. These data reinforce the visual impression that on scales less than ~ 30 Mpc there is a tendency for clusters in our sample to point towards their nearest neighbour. That we find one cluster with $D \sim 6$ Mpc and $\theta \sim 83°$ does not detract from this general conclusion. For perfect alignment one would expect $\sigma \sim 1$. If clusters are distributed in a cell structure as suggested by Dekel, West and Aarseth (1984, see in particular their Figs. 2 and 3a) one would not expect perfect alignment to occur. One would expect several strongly aligned clusters $\theta \leq 30°$ and a few strongly nonaligned clusters which is in fact just what we see. The amount of disagreement on various scales is an indication of the scale of the cell structure and where in this structure the clusters lie. This should be a subject for further study.

5. Conclusion

We have defined a method for determining the position angle of elongation of Abell clusters, taking into account the significance of the position angle. We have compared our data with those of Binggeli and Struble & Peebles. We have shown that statistically the position angle differences are correlated with the strength of elongation signal in a sample of Abell clusters. We confirm the alignment of first ranked galaxy with cluster elongation, indeed we find a stronger effect than that found by Binggeli. With our limited subsample of Binggeli's sample we confirm that the tendency for a cluster to point to its nearest neighbour is present although at a weaker level than that found by Binggeli. As we remove the more weakly elongated clusters from the sample the effect gets stronger but better statistics are needed to confirm this. We intend to apply this method to a larger sample of Abell clusters.

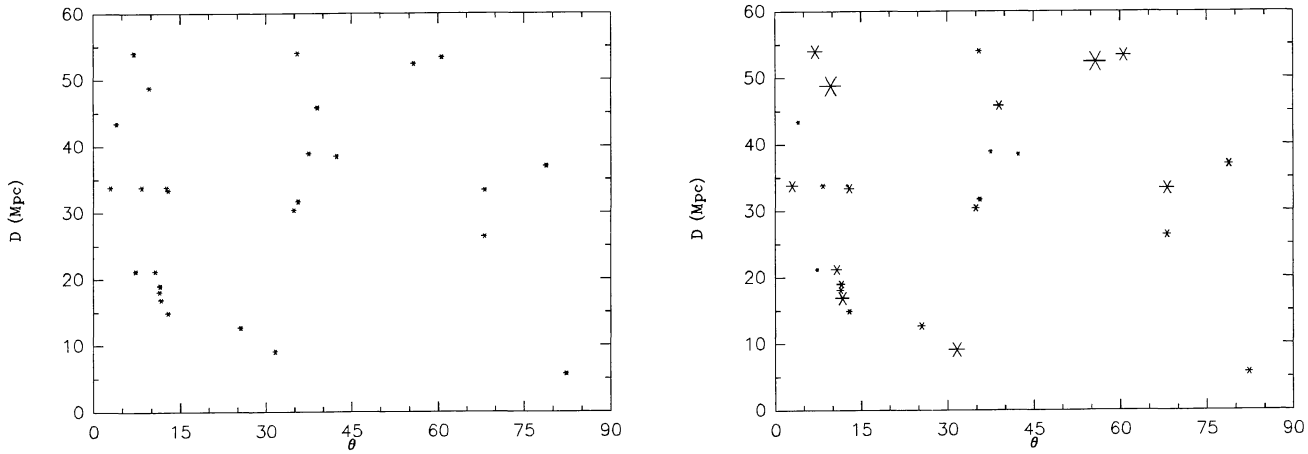

Fig. 6. a The difference (θ) between the cluster position angle and the position angle defined by the direction to the closest neighbouring cluster, versus the spatial distance to the closest neighbouring cluster. **b** The same as **a** except the symbol size is proportional to the cluster elongation strength

Acknowledgements. We thank Professor J.H. Oort for his active interest in this study, Dr. C.P. de Vries for supplying the essential building blocks for the digital image analysis software and Professor C. van Schooneveld for discussions concerning the statistics of position angle determination. We thank the referee, Dr. G. Chincarini for his careful reading of the manuscript and his useful suggestions. G.F.R.N. Rhee acknowledges support from the Netherlands Foundation for Astronomical Research (ASTRON) through grant #782-373-036.

References

Argyres, P.C., Groth, E.J., Peebles, P.J.E.: 1986, *Astron. J.* **91**, 471

Binggeli, B.: 1982, *Astron. Astrophys.* **107**, 338

Carter, D., and Metcalfe, N.: 1981, *Monthly Notices Roy. Astron. Soc.* **191**, 325

Dekel, A., West, M.J., Aarseth, S.J.: 1984, *Astrophys. J.* **279**, 1

Dressler, A.: 1978, *Astrophys. J.* **226**, 55

Geller, M.J., Beers T.C.: 1982, *Publ. Astron. Soc. Pacific.* **94**, 421

Kron, R.G.: 1980, *Astrophys. J. Suppl.* **43**, 305

Minkowski, R.L., Abell G.O.: in *Stars and Stellar Systems* Vol III (ed K.A. Strand Chicago: University of Chicago Press) (1963) 481

Oort, J.H.: 1983, *Ann. Rev. Astron. Astrophys.* **21**, 373

Sastry, G.N.: 1968, *Publ. Astron. Soc. Pacific.* **80**, 252

Struble, M.F., Peebles, P.J.E.: 1985, *Astron. J.* **90**, 582

Swaans, L.: 1981, Ph.D. Thesis, University of Leiden